

## RESEARCH ARTICLE

10.1029/2023JG007609

## Key Points:

- Lateral flux of dissolved inorganic carbon (DIC) is not well resolved in time and space in Southeast Alaska
- We present robust models for DIC flux on a watershed basis that are spatially and temporally explicit
- Calculated DIC flux from Southeast Alaska watersheds is heavily influenced by streamflow regime and karst presence

## Supporting Information:

Supporting Information may be found in the online version of this article.

## Correspondence to:

J. R. Harley,  
[john.harley@alaska.edu](mailto:john.harley@alaska.edu)



## Citation:

Harley, J. R., Biles, F. E., Brooks, M. K., Fellman, J., Hood, E., & D'Amore, D. V. (2023). Riverine dissolved inorganic carbon export from the Southeast Alaskan Drainage Basin with implications for coastal ocean processes. *Journal of Geophysical Research: Biogeosciences*, 128, e2023JG007609. <https://doi.org/10.1029/2023JG007609>

Received 13 JUN 2023

Accepted 26 SEP 2023

## Riverine Dissolved Inorganic Carbon Export From the Southeast Alaskan Drainage Basin With Implications for Coastal Ocean Processes

John R. Harley<sup>1</sup> , Frances E. Biles<sup>2</sup> , Mariela K. Brooks<sup>3</sup> , Jason Fellman<sup>1</sup> , Eran Hood<sup>1</sup> , and David V. D'Amore<sup>2</sup> 

<sup>1</sup>Alaska Coastal Rainforest Center & Program on the Environment, University of Alaska Southeast, Juneau, AK, USA, <sup>2</sup>Forest Service, U.S. Department of Agriculture, Pacific Northwest Research Station, Juneau, AK, USA, <sup>3</sup>Auke Bay Laboratories, Alaska Fisheries Science Center, National Oceanographic and Atmospheric Administration, Juneau, AK, USA

**Abstract** Dissolved inorganic carbon (DIC) represents an important but poorly constrained form of lateral carbon flux to the oceans. With high precipitation rates, large glaciers, and dense temperate rainforest, Southeast Alaska plays a critical role in the transport of carbon to the Gulf of Alaska (GOA). Previous estimates of DIC flux across the Southeast Alaska Drainage Basin (SEAKDB) are poorly constrained in space and time. Our goal was to incorporate recent measurements of DIC concentrations with previous measurements from the U.S. Geological Survey in order to model the spatial and temporal patterns of riverine DIC transport from SEAK to the GOA. We aggregated DIC concentration measurements from 1957 to 2020 and associated measurements of mean daily discharge. We then constructed load estimation models to generate concentration predictions across 24 watersheds. By spatially matching measurements of DIC with SEAKDB watersheds, we extrapolated concentration predictions across 2,455 watersheds encompassing approximately 190,000 km<sup>2</sup>. Models were aggregated according to two factors, the presence of karst and the discharge regime. Finally, monthly flux predictions were generated for each watershed using predicted concentrations and runoff estimates from the Distributed Climate Water Balance Model. Mean annual DIC flux from the SEAKDB was 2.36 Tg C with an average yield of 12.52 g C m<sup>-2</sup>. Both karst presence and flow regimes modified DIC flux and speciation across coastal marine areas. The high resolution of DIC flux estimates will provide useful inputs for describing seasonal C dynamics, and further refines our understanding of C budgets in the Pacific temperate rainforest and the surrounding marine environment.

**Plain Language Summary** Understanding how carbon moves through ecosystems is critical in a changing climate. Dissolved carbon in aquatic environments plays a critical role in driving large-scale processes such as ocean acidification, which represents a threat to many marine ecosystems. Despite the importance of understanding and accounting for carbon as it moves through the environment, the transfer of dissolved inorganic carbon (DIC) (such as carbon dioxide) from the terrestrial environment to the marine environment is often overlooked. Streams and rivers transfer carbon from land to ocean and represent a significant source of carbon to the marine environment, especially in areas that have large amounts of freshwater discharge such as Southeast Alaska. In this study, we created a model which generates predictions for how much DIC is entering the marine environment of Southeast Alaska. For each of 2,455 watersheds identified in this region we calculated monthly flux estimates which we grouped into large marine zones. Our overall flux estimate agrees well with previous estimates, but here our model provides more highly resolved spatial and temporal flux values which reveals seasonal and geographic patterns of DIC transfer from rivers to the marine environment.

### 1. Introduction

Dissolved inorganic carbon (DIC) is an important component of the global carbon budget, however the role of DIC export from the terrestrial to marine environments is poorly constrained in space and time, making impacts to global processes such as ocean acidification uncertain (Bauer et al., 2013). Sources of DIC in aquatic systems are varied and multi-faceted and include atmospheric dissolution (CO<sub>2</sub> gas exchange), weathering from carbonate-rich lithologies, and heterotrophic respiration in both terrestrial and aquatic ecosystems (Campeau et al., 2017; Guo et al., 2015; Li et al., 2017). Lateral flux of DIC from terrestrial ecosystems via streams and rivers represents a substantial portion (38%) of the annual global lateral flux of riverine carbon to the oceans

(i.e.,  $0.41 \text{ Pg C y}^{-1}$  from DIC, Li et al., 2017). Despite representing a major pathway for carbon in global cycling, riverine DIC transport has only recently been promoted in regional and national monitoring efforts (Butman & Raymond, 2011; Butman et al., 2018; Drake et al., 2018; Raymond et al., 2013).

While changes in global carbon budgets driven by anthropogenic  $\text{CO}_2$  emissions have received international attention, changes in precipitation regimes, cryospheric water and carbon storage, and vegetation coverage also have the potential to affect large-scale inputs of DIC and dissolved organic carbon (DOC) to fluvial networks (Guo et al., 2015; Tank et al., 2012). In the Arctic, landscape changes such as melting permafrost have been shown to cause increased sulfide oxidation and DIC mobilization (Tank et al., 2016). Streamwater DIC typically occurs in higher concentrations than DOC; however, DIC which consists of multiple carbonate species is more difficult to measure directly, resulting in less available data and fewer modeling efforts across larger regions (Jarvie et al., 2017; Li et al., 2017; Stackpoole et al., 2017).

Oceanographers, fisheries managers, and stakeholders in many coastal areas share a particular concern in assessing the ecosystem impacts of alterations in marine carbonate system equilibria. Such alterations are, to a large extent, due to increases in temperature and changes in the frequency of extreme precipitation events. Both of these have the potential to impact ocean acidification, a process largely driven by marine uptake of anthropogenic  $\text{CO}_2$  which causes shifts in DIC equilibrium, though the relationship is more complex in coastal ecosystems as compared to the open ocean (Bates et al., 2012; Doney et al., 2009; Duarte et al., 2013; Savoie et al., 2022). Model simulations with increasing DIC concentrations in freshwater ecosystems have been shown to impact coastal acidification processes by altering pH both locally at estuarine interfaces of large rivers and more broadly across ocean basins (Bianucci et al., 2018; Gomez et al., 2021; Savoie et al., 2022). The pH of seawater affects the equilibrium of aragonite (a form of calcium carbonate- $\text{CaCO}_3$ ) and bicarbonate ( $\text{HCO}_3^-$ ), such that the shells of calcium carbonate shelled organisms become difficult to form at aragonite saturation states ( $\Omega_A$ )  $< 1$  (Orr et al., 2005). This can directly affect the development, growth, and recruitment of important commercial, recreational, and subsistence shellfish species (Punt et al., 2014). Several studies have examined ocean acidification conditions under various  $\text{CO}_2$  emission scenarios (e.g., Steinacher et al., 2009). However, as a major source of dissolved carbon into the marine system, it is critical to understand and quantify local and regional carbon flux from freshwater sources (Siedlecki et al., 2017).

A previous effort to model freshwater DIC flux in Alaska grouped Southeast Alaska (SEAK) and its transboundary rivers into a single hydrologic unit named “Southeast Region” (Stackpoole et al., 2016, 2017). Stackpoole et al. (2016) estimated an annual average of  $2.6 \text{ Tg C}$  as DIC is transported laterally from Southeast Region streams to the Gulf of Alaska (GOA). Despite the Southeast Region having the lowest average DIC concentration across the state, the regional flux to the GOA was one of the largest sources of DIC per unit area in the state. The high rates of lateral flux of DIC in SEAK is largely due to the high rates of runoff driven by glacial mass loss and high precipitation rates (Stackpoole et al., 2017). Recently, total DOC flux from the source-to-sea watersheds that comprise the Southeast Alaska Drainage Basin (SEAKDB), an area similar in extent to Stackpoole et al.’s (2016) Southeast Region, was estimated at  $1.17 \text{ Tg C y}^{-1}$  (Edwards et al., 2021). However lateral carbon fluxes are dominated by DIC at the coastal margins in Southeast Alaska (Stackpoole et al., 2017), thus it is essential to also understand the dynamics of DIC for developing and constraining terrestrial carbon budgets. With the development of smaller-scale watershed estimates for DOC flux across the SEAKDB (Edwards et al., 2021), we can more accurately constrain lateral carbon budgets with the incorporation of DIC flux estimates on this scale.

While the approach from Stackpoole et al. (2017) provided a comprehensive carbon flux estimate based on observed discharge and stream chemistry data, their DIC model was constrained in time and space to a single annual estimate for the Southeast Region as a whole. In this paper, we present an expanded model that refines the temporal and spatial variability of DIC across the landscape in the following ways. First, we produced monthly estimates of stream DIC concentrations and lateral fluxes. Second, we refined the spatial variability of DIC concentration across the landscape by accounting for regional lithology. And lastly, we provided DIC flux estimates at the watershed level to highlight sub-regional patterns. The ability to identify zones of concern or community vulnerability with respect to ocean acidification or other coastal processes is hindered by the lack of spatial and temporal trends of terrestrial carbon flux across the diverse landscape of the SEAKDB. Oceanographers often rely on flow and constituent loads only from major rivers to predict freshwater and alkalinity flux to the coastal ocean (e.g., Hauri et al., 2020). However, the presence of varying flow regimes and landscape heterogeneity creates widely varying patterns of carbon export, and these patterns are obscured if only major rivers are

accounted for (Edwards et al., 2021). In this study, our goal was to incorporate recent measurements of stream DIC concentrations from the Juneau, Alaska area with historic and ongoing measurements from the U.S. Geological Survey (USGS) to model the spatial and temporal patterns of riverine DIC transport from SEAK to the GOA. We utilized monthly freshwater discharge, measured streamwater DIC concentration, and spatially explicit flux estimates to predict monthly DIC flux on scales relevant to local oceanographic and ecologic processes.

## 2. Methods

A roadmap of our approach is presented here with further detail on each step presented in subsequent sections. First, we gathered applicable DIC and discharge data from the region and created models predicting DIC concentrations from streamflow for 24 watersheds. We classified each watershed in the SEAKDB by discharge regime and karst presence; then we used concentration models for each regime/karst type to predict average monthly flux estimates using modeled monthly discharge estimates based on climate normals. Finally, we calculated spatially explicit estimates for outflow for each watershed in order to aggregate flux estimates into relevant marine zones.

### 2.1. Study Area

The SEAKDB includes all the coastal watersheds of SEAK north of Dixon Entrance and south of Yakutat Bay, with approximately 54% of the watershed contributing area lying in the Canadian provinces of British Columbia and the Yukon Territory (Figure 1; Edwards et al., 2021). The SEAKDB contains a large portion of the north-east Pacific coastal temperate rainforest as well as significant glacial cover. More than 40% of the freshwater input into the GOA comes from the SEAKDB (Edwards et al., 2021; Neal et al., 2010), with seasonal discharge patterns associated with snowmelt, glacier melt, and rainfall (Curran & Biles, 2021). Watersheds range from steep coastal ephemeral streams to massive glacial transboundary rivers such as the Stikine, Taku, and Alek rivers. Annual precipitation is generally intense and abundant but displays variable patterns across the region, ranging from an average of >5,000 mm of precipitation annually in the southern SEAKDB mostly as rain, to <700 mm in parts of the northern SEAKDB (Shulski & Wendler, 2007), and <300 mm annually in some inland areas (Wang et al., 2012). Precipitation is also modified heavily by extensive coastal mountain ranges, with significant amounts falling as snow at higher elevations (Shulski & Wendler, 2007).

To estimate DIC fluxes for the SEAKDB we used an existing geographic information system (GIS) dataset that included 2,455 watershed polygons (Biles et al., 2021). These watershed polygons were derived from the U.S. Watershed Boundary Dataset HU12 level watersheds (Watershed Boundary Dataset (WBD), 2012) and the British Columbia Freshwater Atlas (British Columbia Ministry of Forests, Lands, Natural Resource Operations and Rural Development, 2012) and then were merged to depict whole source-to-sea basins. Small (<40.5 km<sup>2</sup>) watersheds draining the coastal fringe that did not meet the HU12 minimum mapping size were lumped into single watershed units up to approximately 162 km<sup>2</sup>. For flux calculations, these lumped units are treated identically to traditional, single-outlet watersheds.

### 2.2. DIC Concentrations

Concentrations of DIC were calculated from alkalinity as CaCO<sub>3</sub> (ALK), temperature (TEMP), and pH measurements obtained from two sources. First we obtained data from the USGS National Water Information Service (NWIS; U.S. Geological Survey, 2023) from 1949 to 2020 using the R package *dataRetrieval* (1,268 samples from 286 locations; De Cicco et al., 2018; R Core Team, 2023) which comprised largely the same data used by Stackpoole et al. (2016). Data in this initial set included concurrent measurements of ALK, TEMP, and pH (parameter codes 00410, 00010, and 00400) from USGS sites located within the bounds of the SEAKDB (green dots in Figure 1). As in Stackpoole et al. (2016) we removed observations with pH < 5.6 due to the potential for organic acids to contribute non-carbonate alkalinity (total of 32 samples excluded, Abril et al., 2015; Driscoll et al., 1989). Total DIC measurements were also extracted from NWIS (parameter code 00691) from watersheds within the bounds of the SEAKDB resulting in 56 additional samples from eight locations from 2019 to 2020.

The second source of DIC concentrations were measurements of stream chemistry we collected from five rivers (Cowee Creek, Fish Creek, Peterson Creek, Herbert River, and Mendenhall River, see Figure S1 in Supporting Information S1) along the Juneau, Alaska road system (henceforth JRS) from 2015 to 2020 ( $n = 430$ , Harley

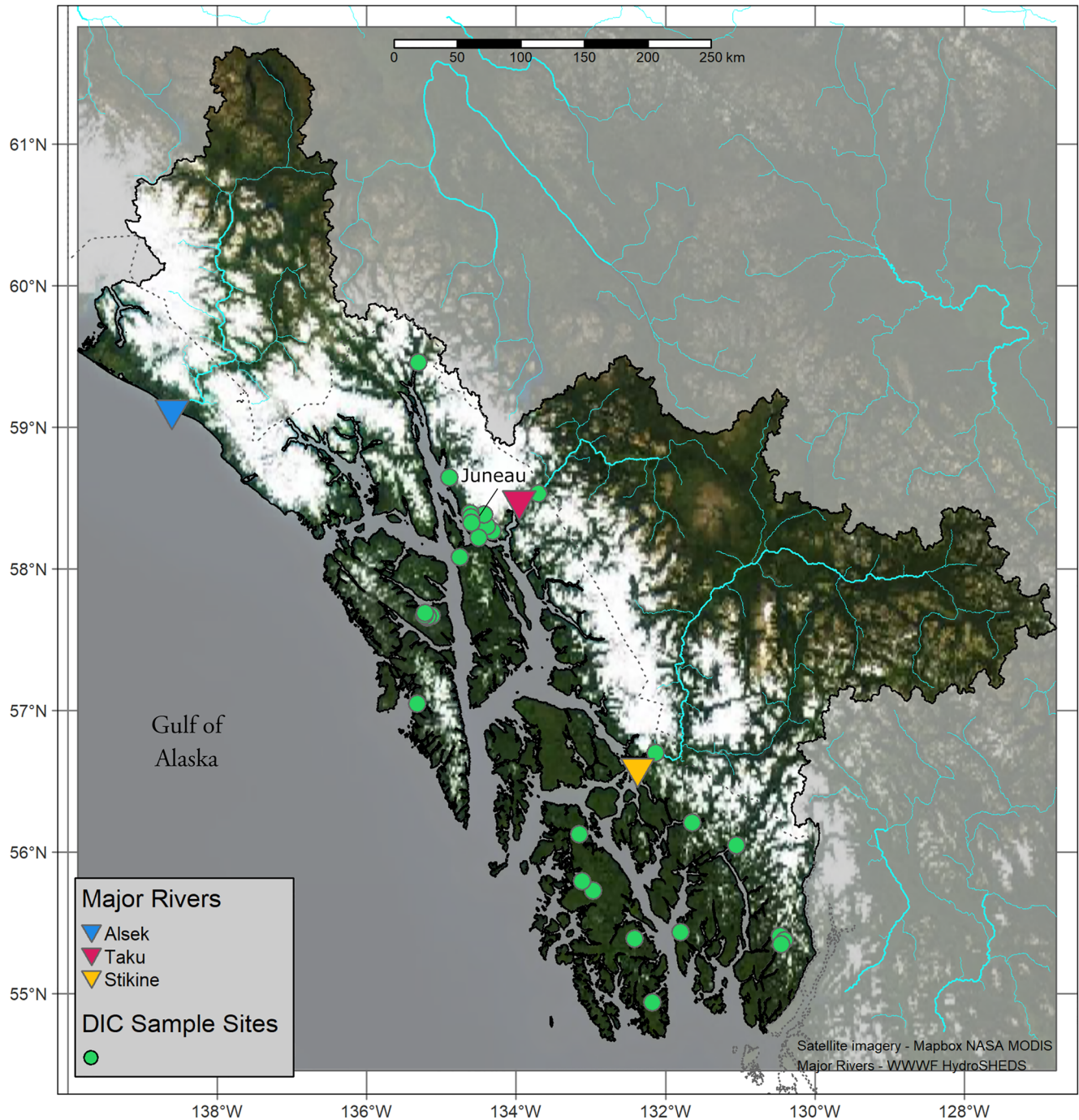
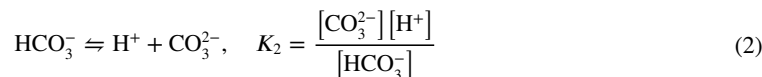
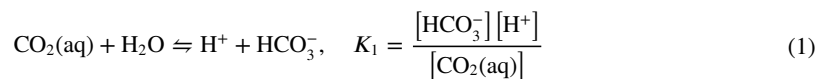


**Figure 1.** The Southeast Alaska Drainage Basin (SEAKDB) and dissolved inorganic carbon (DIC)/discharge sample locations (green dots). The mouths of three major transboundary rivers are shown as colored triangles—these and other major river systems are displayed in cyan. The dotted line shows the approximate location of the U.S.-Canada border.

et al., 2022). For these samples, alkalinity was measured unfiltered as  $\text{CaCO}_3$  in  $\text{mg L}^{-1}$  by titration to two pH endpoints (pH 4.7 and 4.4) using 0.02 N hydrochloric acid. Streamwater pH was measured using field temperature-calibrated digital probes (Accumet ATC or Orion Star ATC) and temperature was measured to the nearest tenth  $^{\circ}\text{C}$  using a hand-held YSI multi-parameter unit.

DIC was calculated from ALK, TEMP, and pH using the *seacarb* package with dissociation constants ( $K_1$  and  $K_2$ ) from Waters et al. (2014) described in Equations 1 and 2 (Gattuso et al., 2018).



DIC observations were matched to SEAKDB watershed polygons by selecting the polygon which contained the latitude and longitude of the sampling site or station, or in a small number of cases the nearest polygon to the sampling site. In two instances where large rivers (Taku and Stikine) have created wide coastal deltas, sampling sites corresponded to incorrect polygons, however based on the sample metadata and local knowledge we manually reassigned these samples to the correct basins.

### 2.3. Discharge Measurements

For the JRS watersheds, discharge in Cowee and Fish Creeks were measured at 15-min intervals for the 2015–2020 JRS study period using a stilling well equipped with a pressure transducer (in situ troll). Discharge measurements ( $n > 15$ ) were made across a wide range of stage to derive the stage-discharge relationship used to calculate mean daily discharge. Discharge for Peterson Creek for 2018–2020 was collected using the same methodology. For the 2015–2017 period, Peterson Creek discharge was obtained from the Alaska Department of Fish and Game (Sowa, 2013). Herbert River discharge was modeled using flow obtained from NWIS for the nearby and similar Mendenhall River (USGS site# 15052500). The Herbert River regression model is described in Hood et al. (2020, section 2.3), which is highly correlated to the Mendenhall across a 5-year period of overlap (see Hood et al., 2020 for detail). Mendenhall River streamflow data for 2015–2020 was obtained from the USGS using the R software dataRetrieval package (De Cicco et al., 2018). The discharge data for Cowee, Fish, Peterson, and Herbert can be found in Harley et al. (2022).

### 2.4. Modeled Discharge Estimates

We obtained estimates of mean monthly discharge for each SEAKDB watershed polygon from the Distributed Climate Water Balance Model (DCWBM) used in Edwards et al. (2021) and available from GitHub (<https://github.com/jwtrubil/DCWBM>). Briefly, the DCWBM is based on the USGS Thornthwaite monthly water balance model program originally written by McCabe and Markstrom (2007), then modified by Moore et al. (2012) to account for environmental conditions and geospatial input datasets specific to British Columbia, Canada. Edwards et al. (2021) revised Moore et al.'s (2012) implementation to apply the DCWBM to the entire GOA drainage basin, which includes the SEAKDB. To drive the DCWBM, Edwards et al. (2021) used ClimateWNA (Wang et al., 2012) to estimate 1981–2010 temperature and precipitation normals over a 400 m grid, and used European Space Agency GlobCover data (Arino et al., 2012) to assign land cover. The DCWBM was calibrated for the GOA region using measured discharge from 72 streams, each with at least 10 years of streamgage data from the 1981–2010 period. The final model had a median Nash-Sutcliffe efficiency (Nash & Sutcliffe, 1970) of 0.78 for predicting mean monthly discharge across the 72 gaged streams (see Edwards et al., 2021 for additional calibration details). After nearest-neighbor interpolation from 400 to 50 m grid cells, monthly runoff values were aggregated for each SEAKDB watershed polygon (Edwards et al., 2021).

To examine the influence of streamflow regimes on DIC flux dynamics we classified each SEAKDB watershed according to seasonal discharge patterns. We performed a principal component analysis (PCA) on mean monthly DCWBM discharge as a ratio of mean annual discharge (Pardé coefficients; Parde, 1933) and the percent glacier cover (see Section 2.5) of each watershed (13 total variables). Naïve hierarchical clustering was performed using Ward's minimum variance method to generate discharge regime clusters based on seasonal discharge patterns (*hpc* function from the *FactoMineR* package, Lê et al., 2008).

### 2.5. Glaciology and Lithology

Percent glacier cover was calculated for each SEAKDB watershed using the Randolph Glacier Inventory (v.6, Arendt et al., 2017). Area of glacial coverage was divided by the total watershed area to calculate a single percentage for each watershed polygon.

To explore the role of carbonate-rich sediment on DIC concentrations we examined karst cover in the SEAKDB. A GIS dataset showing known karst formations in SEAK (USDA Forest Service, Tongass National Forest, 2021) was merged with a British Columbia, Canada dataset of potential karst areas (British Columbia Ministry of Forests, Lands, Natural Resource Operations and Rural Development, 2002, and described in Stokes & Griffiths, 2019). The British Columbia karst map does not distinguish between known karst deposits and potential karst, consequently the percent coverages for transboundary rivers may not be directly comparable. Therefore, instead of examining karst cover as a continuous variable for modeling we categorically divided watersheds into those without known or potential karst (“no karst”) and those with >0% known or potential karst cover (“karst”). A karst dataset was not available for the Yukon Territory, Canada, where the headwaters of the Alsek River are located; however, the Alsek has known karst in its lower (within Alaska) reaches (USDA Forest Service, Tongass National Forest, 2021). For modeling purposes, its classification would not be affected by the lack of karst mapping in the Alsek headwaters.

## 2.6. DIC Concentration Model and Calibration

From the original pool of 1,754 DIC observations from the USGS and JRS, we selected streams and rivers that had more than 10 DIC measurements and had more than 1 year of continuous daily mean discharge values. This left us with a final pool of 1,288 DIC measurements from 24 watersheds.

Measured stream DIC concentrations and associated discharge values from the 24 watersheds were used to generate predictive concentration models using the R package *rloadest* (based on LOADEST, Runkel et al., 2004). We also incorporated functions from the *loadflex* package (Appling et al., 2015) which allowed us to generate a composite model which corrects for biases in LOADEST regressions by interpolating prediction residuals and adding the resulting interpolated residuals to the predicted values (Appling et al., 2015). Model selection within *rloadest* was performed by minimizing Akaike information criteria values using functions built into *rloadest*. Q-q plots were examined to assess goodness of fit and skewness of the resulting concentration-flow models. Error propagation was incorporated using *loadflex* in estimates of DIC concentrations. Models produced were evaluated using adjusted maximum likelihood estimation (AMLE) regression.

Following model construction, the observations of mean daily discharge without an associated DIC measurement were used as model input to generate predicted DIC concentrations. This resulted in 277,000 mean daily DIC concentration estimates across 24 watersheds.

## 2.7. Computation of Watershed Flux

DIC concentration estimates obtained for the 24 watersheds were aggregated by karst coverage (*karst* vs. *no karst*) and discharge regime (as determined by hierarchical clustering) which resulted in six models. Concentrations were further aggregated by month within each group to generate mean, upper, and lower quantile estimates for DIC concentrations within each discharge regime and karst group (six groups).

These modeled monthly concentration estimates (mean, upper, and lower quantiles) for each karst group and discharge regime were then extrapolated to all watersheds in the SEAKDB ( $n = 2,455$ ). Watersheds were classified by discharge regime (Section 2.3) and karst coverage (Section 2.5), then mean monthly discharge estimates from the DCWBM were multiplied by the appropriate average monthly DIC concentration for that discharge regime and karst group. This resulted in average, lower, and upper DIC flux estimates for each watershed.

Total mean monthly and annual flux values for the SEAKDB were calculated by summing flux estimates across all watersheds. DIC yield for individual watersheds and zones (see Section 2.8) was calculated by dividing the annual flux by the total area for each watershed or zone.

## 2.8. Flow Routing of DIC Flux to Marine Zones

A GIS layer for marine zones was obtained from the National Weather Service (U.S. Department of Commerce, 2023, version *mz08mr23*) and clipped to include zones adjacent to the SEAKDB. These marine zones are generally used for coastal forecasting but are also defined by large geographic features that coincide with distinct marine environments such as fjords and channels (Weingartner et al., 2009).

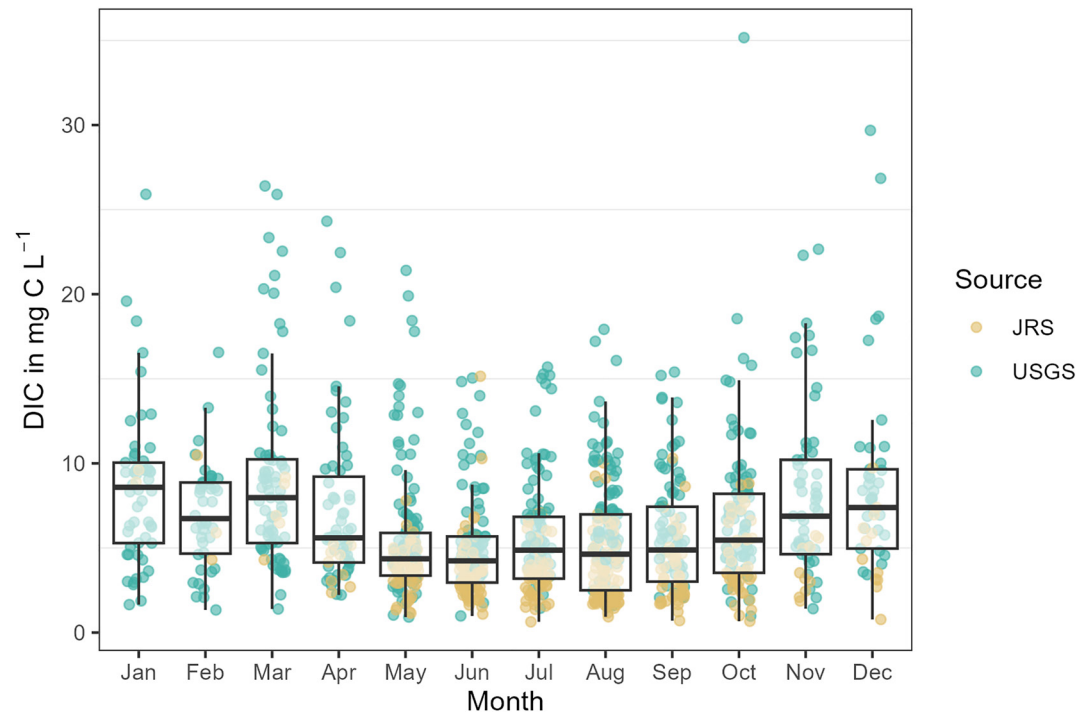


**Figure 2.** Dissolved inorganic carbon (DIC) concentrations grouped by calendar month from two sources, the United States Geologic Survey (USGS) reported in National Water Information Service (NWIS) and data collected in this study along the Juneau Road System (JRS).

To provide flux estimates on geographic units relevant to oceanographers as well as fisheries and ecosystems managers, we aggregated watersheds into marine zones using digital elevation models (DEMs) from the Shuttle Radar Topography Mission (SRTM GL1) Global 30 m Ellipsoidal (OpenTopography, 2020). DEMs were clipped to each SEAKDB watershed polygon. We attempted to find an average outflow point for each watershed by extracting low elevation points for each polygon (<2 m) and spatially averaging their location (centroid). For most watersheds this resulted in a location at river mouth or in some cases a tidewater glacier. For smaller watersheds with multiple outflows into the marine environment this single point represented the average location of outflows. Average centroids for each watershed were then matched to their closest marine zone polygon using Haversine distance.

### 3. Results

#### 3.1. DIC Concentrations

In addition to data from the USGS, our analysis included high temporal resolution JRS samples across a 5-year period (Figure 2, Harley et al., 2022). Median DIC concentration in these five streams (Cowee, Peterson, Herbert, Fish, Mendenhall) was  $5.33 \text{ mg C L}^{-1}$  (95% CI  $1.8\text{--}16.0 \text{ mg C L}^{-1}$ ) which agrees well with the  $5.3 \text{ mg C L}^{-1}$  reported in Stackpoole et al. (2017). Generally, DIC concentrations were inversely related to discharge, and concentration-discharge curves (C-Q) between DIC and scaled discharge show an exponential decay (Figure S2 in Supporting Information S1). Concentrations of DIC were generally lowest in summer months (May–August) during peak discharge for most watersheds in the SEAKDB, while concentrations were highest in winter (December–March) when flows are generally low across regime types.

#### 3.2. Discharge Regime Clustering

The naïve hierarchical clustering of watersheds based on DCWBM runoff and glacier cover resulted in three clusters (Figure 3a and see Figure S3 in Supporting Information S1) corresponding to three distinct flow regimes with different dominant seasonal streamflow drivers. We classified these as “glacial,” “snow and rain,” and

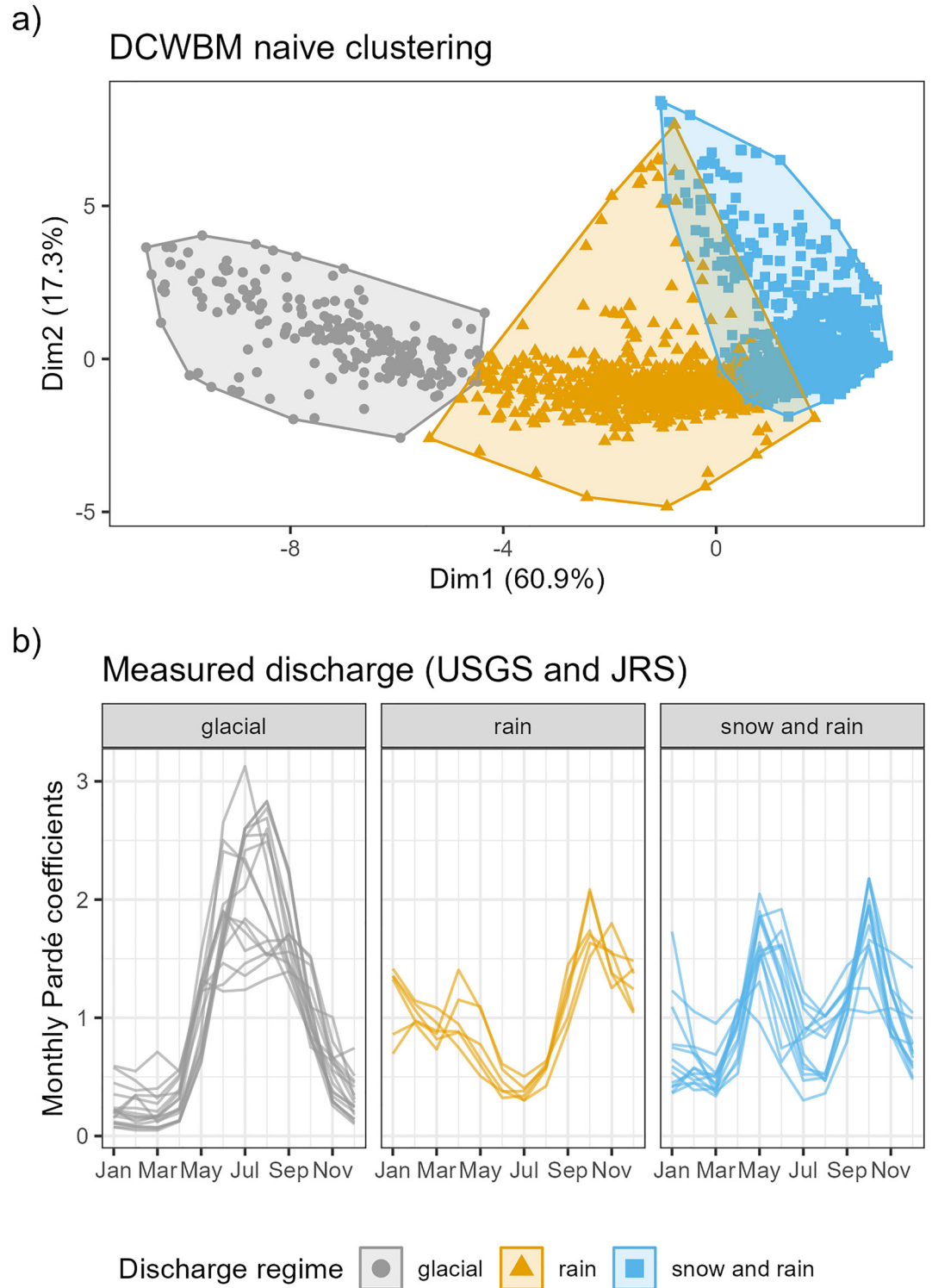


**Figure 3.** (a) Results of clustering based on Ward's distance algorithm using monthly Pardé coefficients of discharge from Distributed Climate Water Balance Model (DCWBM) and glacier cover; (b) monthly Pardé coefficients from in situ measurements are displayed here classified by clustering from the previous panel.

“rain” accordingly (Figure 3b; Curran & Biles, 2021; Sergeant et al., 2020). Glacial regimes exhibit low winter streamflow, a prolonged summer melt period with high flows, and typically (though not always) occur in watersheds with glaciers (Curran & Biles, 2021). Snow and rain regimes contain both a notable spring snowmelt pulse



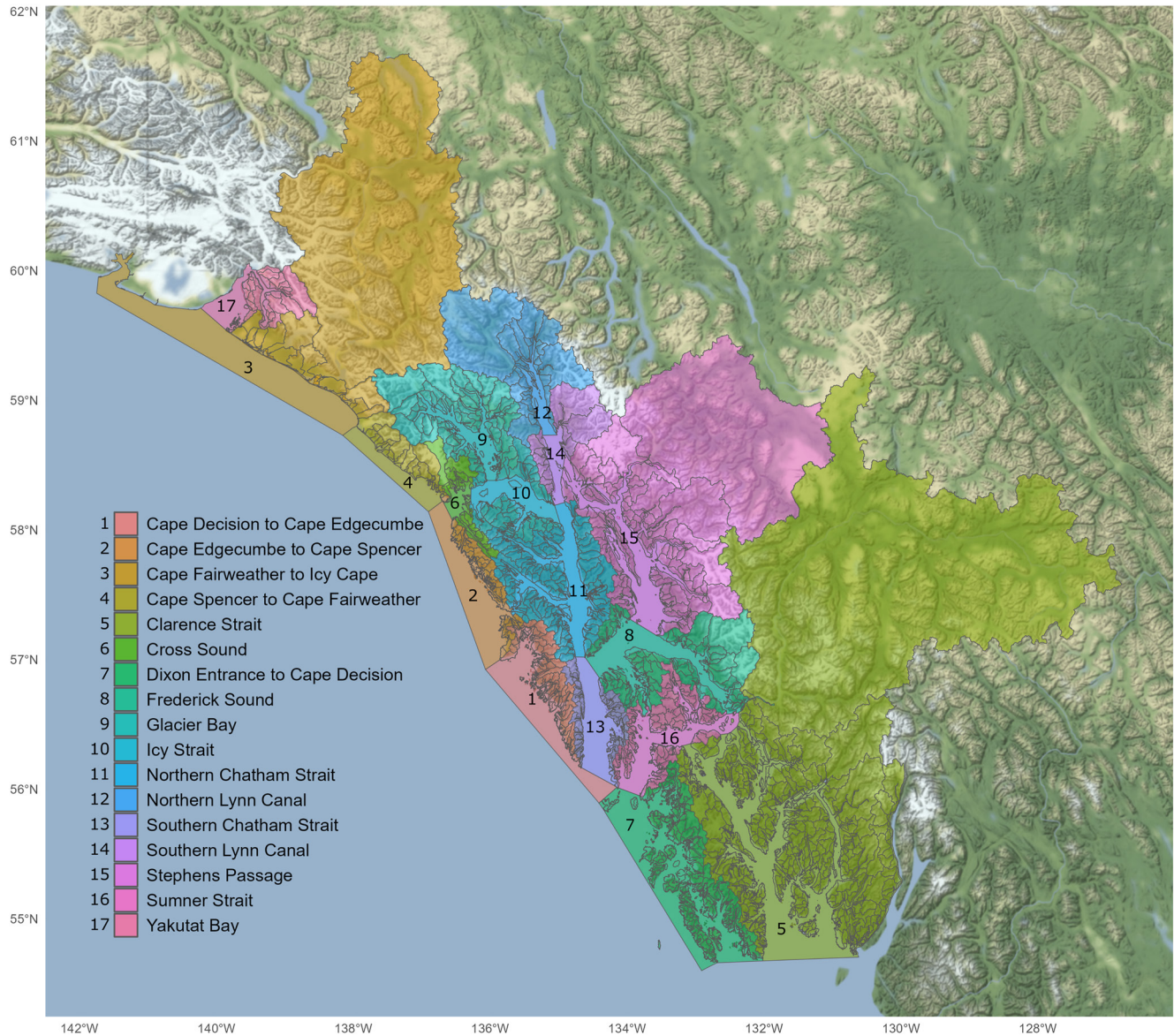


**Figure 4.** Result of spatial associations between Southeast Alaska Drainage Basin (SEAKDB) watersheds and their catchment marine zones as defined by the National Weather Service. Note that three marine zones (Cape Fairweather to Icy Cape, Clarence Strait, and Yakutat Bay) have freshwater inputs which are outside of the defined SEAKDB, thus the calculated flux is an underestimation of the true flux for these zones.

and a fall rain-driven pulse with lower flows in summer and winter. Rain regimes generally mirror the regional precipitation pattern, with highest streamflow in the fall, a notable summer low-flow period, a higher proportion of annual flow occurring in winter compared to other regimes, and occasionally a small spring snowmelt pulse.

### 3.3. Marine Zones

Aggregated low elevation points for each watershed were spatially matched to National Weather Service (NWS) marine zones, the results of which are shown in Figure 4. For small watersheds (e.g., area <40 km<sup>2</sup>) which aggregated multiple subbasins along a coastal fringe (see Edwards et al., 2021), the averaged single low point was often inland, reflecting multiple smaller point sources across a complex geometry. However, in almost every case the subbasins of these aggregated watersheds all drained into a single marine zone which was accurately matched to the low point estimate by spatial proximity. In initial spatial association, the Stikine River was grouped into Frederick Sound. However, based on local knowledge and satellite imagery which clearly

**Table 1**  
Results of Spatial Associations From SEAKDB Watersheds to Marine Zones

Marine zone	Marine zone SA (km <sup>2</sup> )	Contributing terrestrial discharge (km <sup>3</sup> y <sup>-1</sup> )	Depth of annual discharge over marine zone SA (m y <sup>-1</sup> )
Cape Decision to Cape Edgecumbe	3,300	10.37	3.14
Cape Edgecumbe to Cape Spencer	3,188	4.86	1.52
<i>Cape Fairweather to Icy Cape</i>	5,940	67.08	11.29
Cape Spencer to Cape Fairweather	1,385	10.07	3.14
<i>Clarence Strait</i>	8,804	128.30	14.57
Cross Sound	504	7.03	13.95
Dixon Entrance to Cape Decision	5,839	11.93	2.04
Frederick Sound	2,983	20.79	6.97
Glacier Bay	1,315	25.58	19.45
Icy Strait	1,376	6.23	4.53
Northern Chatham Strait	2,619	17.79	6.79
Northern Lynn Canal	669	19.82	29.64
Southern Chatham Strait	2,339	5.91	2.53
Southern Lynn Canal	724	10.15	14.01
Stephens Passage	3,212	64.95	20.22
Sumner Strait	2,553	7.10	2.78
<i>Yakutat Bay</i>	1,167	12.09	10.36
Total	147,236	188,829	

Note. Total annual discharge for each marine zone is calculated from the Distributed Climate Water Balance Model (DCWBM). Zones in italics on the fringe of the SEAKDB represent underestimates of freshwater input since the SEAKDB region does not fully encompass all watersheds draining into that marine zone. SA, surface area; SEAKDB, Southeast Alaska Drainage Basin.

illustrated the direction of ocean currents in the vicinity of the river outlet, we manually assigned discharge from the Stikine River and several nearby watersheds on its delta to Clarence Strait, which captures the majority of Stikine River flow.

Annual discharge for each marine zone catchment is presented in Table 1. Marine zones in the inner channels of the Northern SEAKDB (e.g., Northern Lynn Canal) receive a large amount of freshwater input relative to the surface area of their basin, driven largely by the high degree of glacial coverage of these areas (Figure S3 in Supporting Information S1). Marine zones such as Sumner Strait and Southern Chatham are dominated by rain and snow and rain type watersheds and receive relatively low amounts of freshwater input relative to their surface area (2.78 and 2.53 m km<sup>-2</sup> y<sup>-1</sup>).

### 3.4. DIC Flux

AMLE regression models produced by *loadflex* for each of 24 watersheds had mean coefficients of determination ( $R^2$ ) of 0.91 and a percent bias of -0.73%. AMLE regressions were significant for all watersheds ( $p < 0.05$ ) compared to intercept-only models. Nash-Sutcliffe efficiencies for modeled output compared to observed concentrations ranged from 0.58 to 0.99 (mean = 0.81) representing very good model performance across the 24 watersheds.

In most months, concentrations of DIC were significantly higher in watersheds with karst terrain compared to watersheds with no known or suspected karst (Figure 5a, Games-Howell  $p < 0.01$ ). The presence of karst drove higher average concentrations of DIC in both rain and snow and rain watersheds all year (Figure 5a), however concentrations of DIC in glacial systems were in general higher in watersheds with no karst during periods of lower flow (Fall-Spring).

Mean annual DIC flux from the SEAKDB was estimated to be 2.36 Tg C with an average yield of 12.52 g C m<sup>-2</sup> (Table 2). Monthly DIC flux was highest in June–September and lowest in January–March (Table 2). Fluxes of DIC showed a seasonal pattern correlated with discharge in each streamflow regime type and flux was generally higher in watersheds that had karst than

watersheds without, although this pattern was not observed in snow and rain watersheds where total flux was comparable between watersheds with karst and those without karst (Figure 5b).

Seasonal DIC flux patterns into marine basins generally mirrored respective quantity and seasonal patterns of freshwater discharge into each basin. The coastal waters of Clarence Strait received the largest riverine DIC flux followed by Stephens Passage and the outside waters of Cape Fairweather to Icy Cape (Table 3; Figure 6). Overall, large variations in seasonal flux patterns were observed between different marine zones driven largely by differences in regional hydrology (Figure 6).

### 3.5. DIC Species Flux

Total DIC concentrations were separated into constituent species of carbonate equilibrium using the *seacarb* R package (Gattuso et al., 2018). On average, HCO<sub>3</sub><sup>-</sup> represented approximately 74% of total DIC, although there were differences between karst groups across discharge regime. Across all three discharge regimes, the concentrations of HCO<sub>3</sub><sup>-</sup> were generally twice as high as concentrations of dissolved CO<sub>2</sub> within regime type. Concentrations of carbonate ion (CO<sub>3</sub><sup>2-</sup>) were extremely low as expected at moderate pH (note that we excluded samples with pH < 5.6 as described in the methods, further discussion below). When aggregated to marine zones, the ratios of HCO<sub>3</sub><sup>-</sup> to CO<sub>2</sub> were notably higher along the Northern inside waters compared to the outside waters of the Southeast Alaska archipelago (Figure 7).

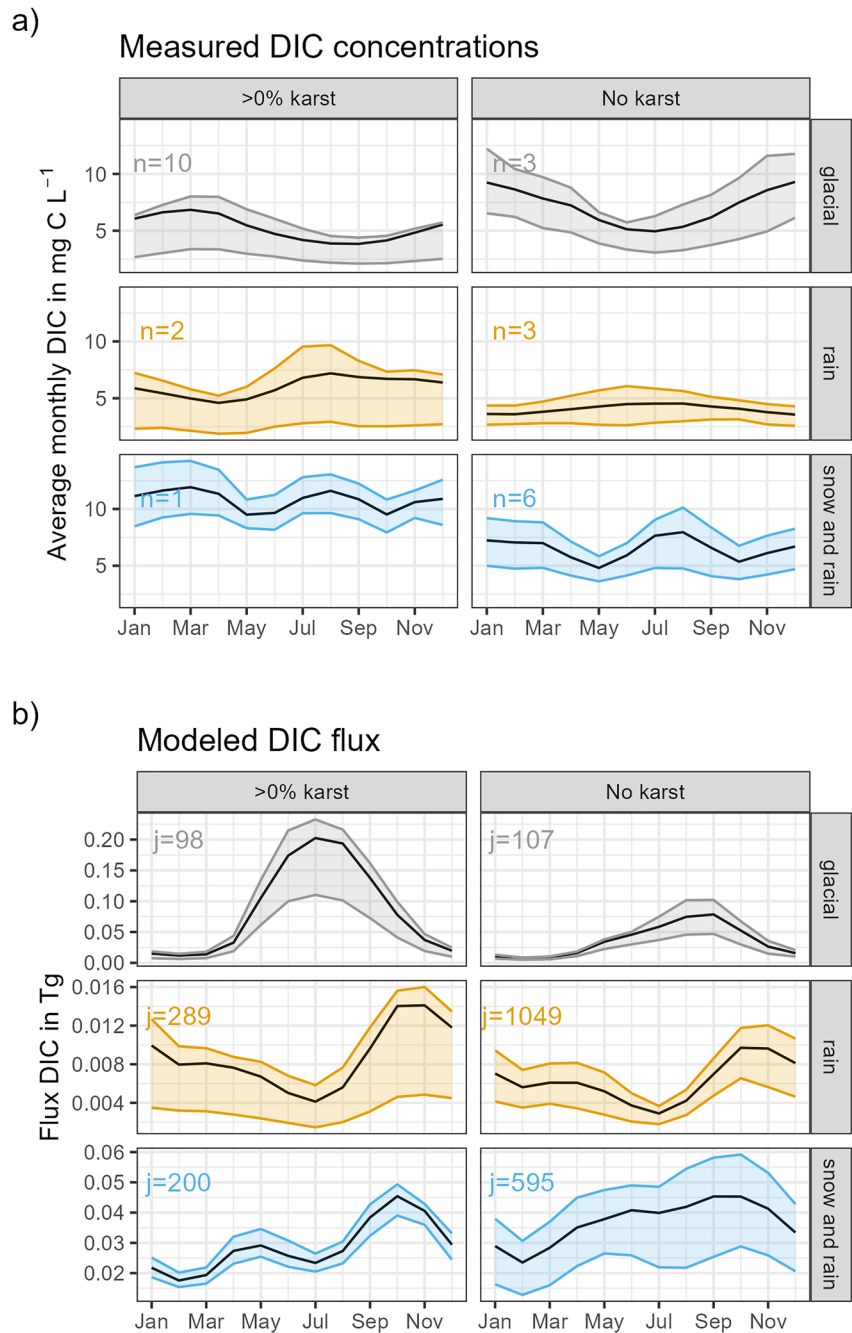


**Figure 5.** (a) Monthly average concentrations of dissolved inorganic carbon (DIC) that were measured in each discharge regime and karst group (95% confidence band is shown as shaded area), where  $n$  represents the number of streams in each group which were used in *loadflex* to create concentration models. (b) Modeled DIC flux for the six groups, showing the average flux as a solid line with 95% confidence bands in shaded area;  $j$  represents the number of Southeast Alaska Drainage Basin (SEAKDB) watersheds in each.

#### 4. Discussion

The flux of terrestrially derived DIC into the marine environment is an important pathway for inorganic carbon transfer that impacts marine or watershed carbon budgeting, coastal ocean acidification, and marine ecosystem function analysis (i.e., carbon sequestration). The land-to-ocean DIC flux is also poorly constrained spatially and temporally in many ecosystems (Jarvie et al., 2017; Tank et al., 2012), making it difficult to identify marine zones of concern with respect to ocean acidification or other coastal processes. Riverine DIC makes

**Table 2**  
Mean Monthly Total Flux and Yield Estimates for SEAKDB

Month	Average DIC flux (Tg C month <sup>-1</sup> )	Range DIC flux (Tg C month <sup>-1</sup> )	Average DIC yield (g C m <sup>-2</sup> month <sup>-1</sup> )	Range DIC yield (g C m <sup>-2</sup> month <sup>-1</sup> )
Jan	0.09	0.06–0.11	0.49	0.31–0.60
Feb	0.07	0.05–0.09	0.40	0.26–0.48
Mar	0.09	0.06–0.11	0.46	0.30–0.56
Apr	0.13	0.09–0.16	0.69	0.46–0.84
May	0.22	0.14–0.27	1.18	0.76–1.43
Jun	0.29	0.18–0.36	1.53	0.96–1.89
Jul	0.32	0.19–0.39	1.67	1.01–2.06
Aug	0.33	0.20–0.40	1.75	1.05–2.14
Sep	0.31	0.18–0.37	1.62	0.98–1.96
Oct	0.24	0.15–0.28	1.27	0.78–1.50
Nov	0.16	0.10–0.19	0.87	0.55–1.03
Dec	0.12	0.07–0.14	0.61	0.39–0.72
<b>Annual</b>	<b>2.36</b>		<b>12.52</b>	

Note. DIC, dissolved inorganic carbon; SEAKDB, Southeast Alaska Drainage Basin. Annual averages are presented in bold at the bottom of the table.

up the majority of lateral carbon transport into the marine environment in the SEAKDB and represents a major source of terrestrial-derived carbon to the GOA (Stackpoole et al., 2016, 2017). For the SEAK region overall, Stackpoole et al. (2016) estimated that DIC comprised 67.2% of the lateral dissolved carbon export. At

finer scales, however, there is variability in DIC:DOC ratios. For example, Edwards et al. (2021) found DOC yields of 16.6 g C m<sup>-2</sup> y<sup>-1</sup> in non-glacial watersheds, which is comparable to mean DIC yields calculated in non-glacial and non-karst watersheds (14.8 g C m<sup>-2</sup> y<sup>-1</sup> as DIC) in our study. In contrast, regions with a dominant glacial freshwater signal have the majority of dissolved carbon as DIC, as concentrations of DOC in glacial watersheds are generally low compared to non-glacial watersheds. DOC yield for glacial watersheds in the SEAKDB region was 2.7 g C m<sup>-2</sup> (including the Alsek, Taku, and Stikine rivers, Edwards et al., 2021) which is roughly 20% of the 10.4 g m<sup>-2</sup> C as DIC calculated here. Glacier-dominated marine zones such as Northern Lynn Canal waters and Glacier Bay are therefore predicted to have a very high DIC:DOC ratio via riverine input, although the fate of this carbon *vis a vis* incorporation into marine carbon processes (photosynthesis, calcification, sedimentation) is difficult to predict (see discussion below).

The three discharge regimes identified here (glacial, snow and rain, rain) are consistent with other studies in the region that used both actual streamflow measurements (Chapman, 1982; Curran & Biles, 2021; Edwards et al., 2013; Shanley & Albert, 2014) and modeled streamflow (Sergeant et al., 2020). It is important to note that while naïve clustering delineates these regimes across the principal components, the discharge regimes exist on a continuum and some watersheds could likely be described by more than one regime type (Figure 3a). As such, other studies have proposed slightly different or more granular classifications for streamflow regimes in Alaska (e.g., Sergeant et al., 2020), our purpose in generating classes was to efficiently analyze potential impacts of watershed type on DIC dynamics. By generating unique models for three flow regimes (in addition to presence/absence of karst) we were able to partition variability in DIC concentrations that might be driven by the associated physical aspects of each regime (i.e., glacial—mechanical

**Table 3**  
Mean Annual Total Flux Estimates by SEAKDB Marine Zones

Marine zone	Average DIC flux (Tg C y <sup>-1</sup> )	Range (Tg C y <sup>-1</sup> )
Cape Decision to Cape Edgecumbe	0.06	0.04–0.08
Cape Edgecumbe to Cape Spencer	0.04	0.03–0.05
Cape Fairweather to Icy Cape	0.32	0.19–0.39
Cape Spencer to Cape Fairweather	0.06	0.04–0.08
Clarence Strait	0.69	0.42–0.83
Cross Sound	0.05	0.04–0.06
Dixon Entrance to Cape Decision	0.06	0.03–0.08
Frederick Sound	0.12	0.08–0.15
Glacier Bay	0.13	0.08–0.15
Icy Strait	0.06	0.04–0.07
Northern Chatham Strait	0.15	0.11–0.18
Northern Lynn Canal	0.09	0.05–0.11
Southern Chatham Strait	0.04	0.03–0.05
Southern Lynn Canal	0.05	0.03–0.06
Stephens Passage	0.33	0.20–0.41
Sumner Strait	0.04	0.03–0.05
Yakutat Bay	0.07	0.04–0.08

Note. DIC, dissolved inorganic carbon; SEAKDB, Southeast Alaska Drainage Basin.

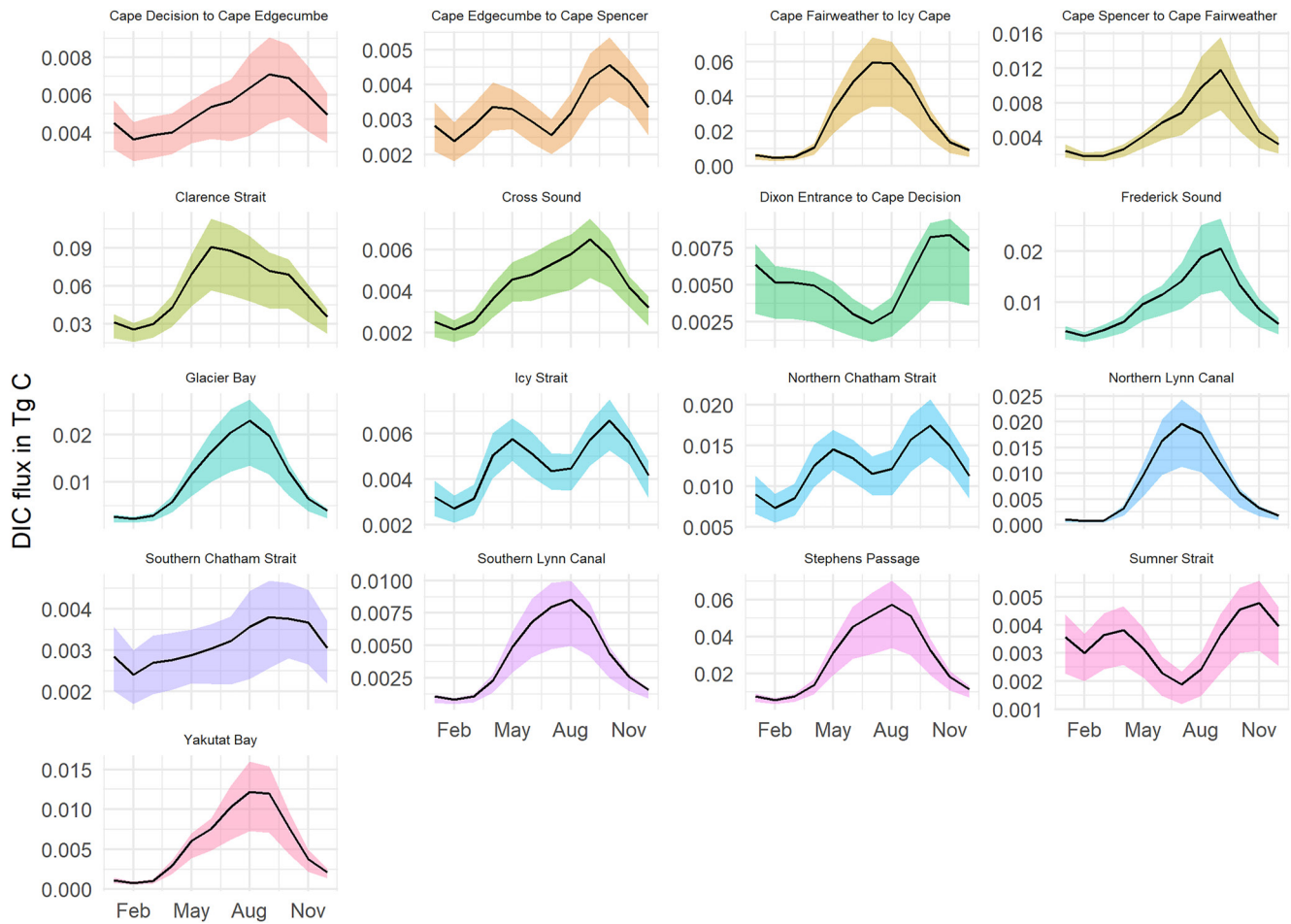


**Figure 6.** Monthly flux values for each marine zone in Southeast Alaska Drainage Basin (SEAKDB). The solid line represents the mean flux estimate for each month, while the shaded region represents the 25th and 75th quantiles for flux estimates.

weathering, rain—wetland respiration). That said, we acknowledge that there are other landscape types and processes that could drive different regime subclasses or DIC chemistry dynamics.

By spatially mapping SEAKDB watersheds to their endpoint marine basin, we can examine patterns of freshwater discharge to the coastal environment. Some inside waters, notably Stephen's Passage and Northern Lynn Canal, receive large amounts of freshwater influx relative to their surface area while other areas such as Sumner Strait and Southern Chatham Strait receive relatively little (Table 1). This can largely be explained by the large amount of glacially influenced watersheds in the northern inside waters of the SEAKDB, compared to the rain and snow and rain watersheds in the southern portion of the region (Figure S3 in Supporting Information S1). It should be emphasized that the results presented in Table 1 are not intended to represent a percentage of the total marine zone volume affected by surface runoff—we do not take into account bathymetry here and the dynamics of estuarine mixing zones are beyond the scope of this paper—however it does emphasize that fluxes of nutrients, elements, or contaminants that are largely driven by discharge (such as DIC) will likely have a higher signal strength in the segments of the marine environment such as Northern Lynn Canal which are heavily influenced by freshwater discharge (Evans et al., 2022).

Our estimate of annual riverine DIC flux from the SEAKDB (2.36 Tg C) agreed closely with Stackpoole et al. (2016, 2017) who reported approximately 2.6 Tg C from DIC was exported laterally to coastal ecosystems from SEAK. This is somewhat expected given the overlap between their dataset and ours, insofar as a large number of USGS (NWIS) water samples are present in both datasets and the additional samples incorporated in this study are within the range reported by Stackpoole et al. (2016). It is also reasonable that our estimate was slightly less than Stackpoole et al.'s (2016). While the boundaries of our SEAKDB region largely overlapped

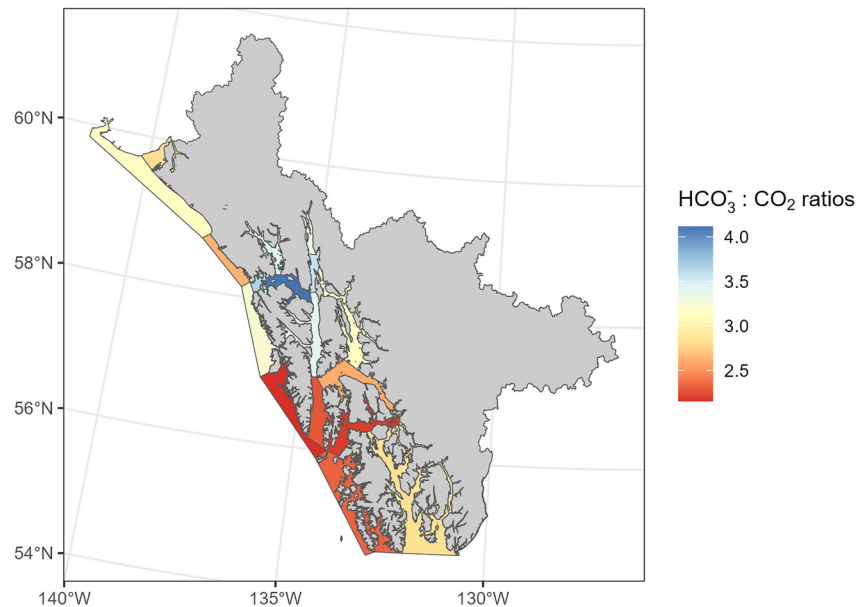


**Figure 7.** (a) Major dissolved inorganic carbon (DIC) species from flux estimates aggregated by marine zones in the Southeast Alaska Drainage Basin (SEAKDB).

with Stackpoole et al.'s (2016) Southeast Region, the Southeast Region contained approximately 9% more area that extended northeast outside the SEAKDB domain. This additional area, which includes a large expanse of mountainous terrain with significant glacier cover, was not included in our assessment. Although estimates of annual DIC flux from SEAK between our study and Stackpoole et al.'s (2016) were comparable, our approaches differed. This study constrained flux estimates within discharge regimes and lithological (karst) features and used monthly modeled runoff from the DCWBM to provide flux estimates at finer temporal (monthly) and spatial (watershed) scales.

Like previous studies we chose to exclude ALK and TEMP observations with  $\text{pH} < 5.6$ .

Average annual DIC yield (flux per unit area) for SEAKDB was  $12.52 \text{ g C m}^{-2}$ , and was highest in snow and rain watersheds with karst present ( $29.91 \text{ g C m}^{-2}$ ), and lowest in glacial watersheds with karst present ( $7.76 \text{ g C m}^{-2}$ , Figures S3 and S4 in Supporting Information S1). The presence of low yields in glacial watersheds with karst is explained by low annual yields from the largest glacial watersheds (i.e., Taku, Alsek, Stikine rivers), which have a dominating influence on this class (Table 4 and Figure S4 in Supporting Information S1).

The average SEAKDB DIC yield reported here is notably lower than the  $24.55 \text{ g C m}^{-2}$  estimated for the Southeast Region by Stackpoole et al. (2016). However, Stackpoole et al. (2016) divided total DIC flux for the Southeast Region by Alaska land area only ( $104,000 \text{ km}^2$ ) instead of the combined contributing land area in Alaska and Canada ( $210,114 \text{ km}^2$ ), resulting in the larger yield value. When Stackpoole et al.'s (2016) total DIC flux estimate of  $2.6 \text{ Tg C}$  is divided by the combined Alaska and Canada area, mean DIC yield is  $12.2 \text{ g C m}^{-2} \text{ y}^{-1}$ , which

is comparable to our estimate. DIC yields reported here were on average substantially higher than those reported for Arctic rivers including the Yukon ( $5.37 \text{ g C m}^{-2} \text{ y}^{-1}$ ) and Mackenzie ( $3.74 \text{ g C m}^{-2} \text{ y}^{-1}$ ) (Tank et al., 2016), consistent with findings showing DIC yields are higher in the temperate latitudes compared to the Arctic (Li et al., 2017; Stackpoole et al., 2017). However, we note that yields for major SEAKDB rivers (Taku, Alsek, and Stikine) were more similar to yields reported in major Arctic Rivers (Table 4).

Like other studies of riverine DIC flux, we found that DIC concentration decreased with increasing streamflow (Figure 2 and Figure S2 in Supporting Information S1) and DIC flux was driven largely by discharge (Prokushkin et al., 2011; Tank et al., 2016). While chemical and mechanical weathering

**Table 4**  
Annual DIC Yields for Three Largest Rivers in SEAKDB

River	Annual DIC flux ( $\text{Tg C y}^{-1}$ )	Total area ( $\text{km}^2$ )	Annual DIC yield ( $\text{g C m}^{-2}$ )
Stikine	0.24	50,831	4.75
Alsek	0.24	28,818	8.26
Taku	0.05	16,808	3.23

Note. DIC, dissolved inorganic carbon; SEAKDB, Southeast Alaska Drainage Basin.

of carbonate minerals represents an important source of DIC in freshwater systems—particularly in the steep, sparsely vegetated, and coastal glacial rivers found in SEAK—the production of CO<sub>2</sub> from respiration of organic materials is an important source of DIC in riverine systems (Campeau et al., 2017; Jarvie et al., 2017). Thus, high flows, while potentially diluting DIC concentrations, could still produce higher fluxes as a result of greater water yields and increased mechanical weathering (Figure 5b). The seasonal flux predictions in Figure 5b emphasize that the total DIC flux for most watersheds and marine zones is more closely related to total discharge rather than the DIC concentrations. While there are other sources of DIC in a system than chemical or mechanical weathering, this finding is consistent with previous work which has shown that the concentration of anion species produced by chemical weathering often do not show a simple dilution relationship with discharge (Godsey et al., 2019) and that total flux on interannual time scales is more closely related to total discharge.

The patterns of seasonal DIC flux to each marine zone (Figure 6) can be largely explained by regional discharge regimes, which are in turn driven by major landscape attributes (i.e., glaciers and elevation) and climate (precipitation and temperature). In general, watersheds with significant glacier coverage (or high elevation snow), such as those found along Clarence Strait and Lynn Canal, have the highest DIC export in July–August in conjunction with peak glacial discharge (Figures 4 and 6). In contrast, regions of rain dominated, lowland watersheds that store little to no seasonal snowpack, such as Dixon Entrance to Cape Decision and Sumner Strait (which does have a small spring snowmelt signal), DIC export and discharge peaks in October–November in conjunction with the highest precipitation rates for SEAK. Also notable in these watersheds is the low summer DIC export, which corresponds to the driest time of the year. Finally, snow and rain watersheds such as those in Icy Strait and Northern Chatham Strait have large spring snowmelt pulses resulting in high discharge rates in May–June and again in October–November during rain events, creating a bimodal pattern of DIC flux over the year.

The influence of glacial runoff on DIC export is apparent in the partitioning of bicarbonate and carbonate ions relative to CO<sub>2</sub> (Figure 7). The NE portion of the SEAKDB has a large glacial extent and experienced a recent (~300 years) glacial advance and alteration of the terrestrial environment (Larsen et al., 2005). Glacial advance increases mechanical weathering of carbonate bearing rock (Guo et al., 2015; Torres et al., 2017) and retreat exposes recently glaciated terrain to increased chemical and hydrologic weathering from increased flows (Anderson et al., 2000; Gislason et al., 2009). How a changing climate will influence the balance between DIC produced from mechanical weathering of glaciers and DIC produced by the chemical and hydrologic weathering of freshly exposed proglacial rock is an intriguing question.

The S and SE section of the SEAKDB has some of the oldest landscapes that were exposed from Pleistocene glaciation 2–4 kya earlier than the northern section (Lesnek et al., 2020). This supports the idea that succession of temperate rainforest across recently deglaciated terrain likely drives the changes to DIC source partitioning from chemical and mechanical weathering to respiration-based processes. In general, decreasing glacial contributions in watersheds leads to increasing primary productivity as water clears and sources of bioavailable carbon increase—which in turn will lead to increased ecosystem respiration (Milner et al., 2017).

Accounting for lateral carbon losses from net ecosystem production is essential for accurately calculating the carbon accretion rate in terrestrial ecosystems. The intense precipitation and exorheic export of elements including carbon from soil and rock in the SEAKDB make estimating inorganic carbon losses a challenging modeling exercise, but a high priority for regional carbon accounting. The DIC loss of 2.36 Tg C is over twice the estimated 1.17 Tg C loss of DOC calculated by Edwards et al. (2021) across the same geographic extent. The combined loss of 3.53 Tg C y<sup>-1</sup> provides a bound on the major lateral export components which until recently was poorly constrained. The coastal rainforests and early successional ecosystems of Alaska and British Columbia are noted for their storage of carbon, with most of this carbon stored belowground (Leighty et al., 2006; McNicol et al., 2019). The annual accretion of carbon has been estimated at 0.01 Mg C km<sup>-2</sup> y<sup>-1</sup>, or an overall accretion rate of 2.67 Tg C y<sup>-1</sup> for the North Pacific temperate region with nearly all of that accretion in soils (2.64 Tg C y<sup>-1</sup>, Genet et al., 2018). This accretion rate is similar to the estimated lateral flux of carbon as DIC we estimated here from the SEAKDB (2.36 Tg C y<sup>-1</sup>), and while carbon accretion in the North Pacific region of Alaska is projected to increase in a changing climate it is unclear how changing climate and landscape use dynamics will affect these lateral carbon flux estimates (Genet et al., 2018). Importantly, our estimates of DIC flux here are calculated at the terrestrial-marine interface and do not take into account dissolved CO<sub>2</sub> evasion along the river networks, which may represent an equal if not larger pathway of carbon transport from terrestrial ecosystems (Stackpoole et al., 2017).

There are several sources of uncertainty in these DIC flux estimates, some of which have been estimated here and others of which are potential sources of bias in our models. Observed variability in DIC concentrations were carried through the flux calculations by incorporating average and quantile concentrations for each of the SEAKDB watersheds. We did not incorporate uncertainty estimates into discharge from the DCWBM; however these monthly discharge estimates represent 30-year normals and comparisons to calibration basins for that model show good Nash-Sutcliffe efficiencies (see supplemental information in Edwards et al., 2021). Nevertheless, on annual scales actual flux of DIC would be largely influenced by more ephemeral variability in discharge, potentially as a result of a rainier than average fall or a hotter than average summer.

While our *loadflex* concentration models showed a very low negative percentage bias, we recognize that excluding low pH samples would potentially bias our flux estimates lower. In systems that are poorly buffered and have low pH, organic acids can contribute significantly to noncarbonate or organic alkalinity (Abril et al., 2015; Driscoll et al., 1989). There were only a small number of samples (32) that were below this cutoff criterion, however, future work could include direct measurements of organic acids to estimate freshwater organic alkalinity in this region and better understand the impacts of acidic, organic-rich freshwaters on coastal ocean acidification.

## 5. Conclusions

Our modeling approach provides a higher degree of spatial and temporal resolution associated with DIC flux estimations than was previously available for the SEAKDB. The more resolved temporal and spatial predictions will reduce some uncertainty in modeling marine chemistry under varying conditions of temperature, salinity, vertical mixing, and nutrient availability (Manizza et al., 2009). This resolution is still quite coarse given the varying terrestrial drivers involved in the production and accumulation of DIC. However, the increased specificity and accumulation into marine zones has allowed us to identify potential areas of vulnerability for increased CO<sub>2</sub> delivery relative to carbonate alkalinity and aggregation into nearshore waters. Further work is clearly needed to resolve these flux estimates into spatial/temporal patterns of ocean acidification in the region including understanding the physical mixing of the freshwater bolus into the nearshore estuary and the dynamics of freshwater derived DIC as it enters the marine environment, however this work provides an important component toward developing a better understanding of these coastal processes in Southeast Alaska. In our flux model, DIC concentrations were determined by discharge regime and karst presence. Although rising global temperatures and precipitation patterns may alter some regime types in the future, at this point future flux estimates could be calculated by using discharge projections from future climate scenarios. This will be especially relevant to communities which rely on fisheries and other marine resources for adaptation planning and food security.

## Data Availability Statement

Stream chemistry measurements, discharge data, and associated metadata from the JRS generated in this study along are available in U.S. Forest Service Research Data Archive (RDA). Harley, J. R., Biles, F. E., Brooks, M. K., Fellman, J. B., Hood, E. W., D'Amore, D. V., 2022. Juneau river stream chemistry and discharge for calculation of inorganic carbon flux [Dataset]. <https://doi.org/10.2737/RDS-2022-0058>.

## References

- Abril, G., Bouillon, S., Darchambeau, F., Teodoru, C. R., Marwick, T. R., Tamooh, F., et al. (2015). Technical Note: Large overestimation of *p*CO<sub>2</sub> calculated from pH and alkalinity in acidic, organic-rich freshwaters. *Biogeosciences*, 12(1), 67–78. <https://doi.org/10.5194/bg-12-67-2015>
- Anderson, S. P., Drever, J. I., Frost, C. D., & Holden, P. (2000). Chemical weathering in the foreland of a retreating glacier. *Geochimica et Cosmochimica Acta*, 64(7), 1173–1189. [https://doi.org/10.1016/S0016-7037\(99\)00358-0](https://doi.org/10.1016/S0016-7037(99)00358-0)
- Appling, A. P., Leon, M. C., & McDowell, W. H. (2015). Reducing bias and quantifying uncertainty in watershed flux estimates: The R package *loadflex*. *Ecosphere*, 6(12), 1–25. <https://doi.org/10.1890/ES14-00517.1>
- Arendt, A., Bliss, A., Bolch, T., Cogley, J., Gardner, A., Hagen, J.-O., et al. (2017). *Randolph Glacier Inventory—A dataset of global glacier outlines: Version 6.0: Technical report*. Global Land Ice Measurements from Space.
- Arino, O., Ramos Perez, J. J., Kalogirou, V., Bontemps, S., Defourny, P., & Van Bogaert, E. (2012). Global land cover map for 2009 (GlobCover 2009) [Dataset]. European Space Agency (ESA) & Université catholique de Louvain (UCL), PANGAEA. <https://doi.org/10.1594/PANGAEA.787668>
- Bates, N. R., Best, M. H. P., Neely, K., Garley, R., Dickson, A. G., & Johnson, R. J. (2012). Detecting anthropogenic carbon dioxide uptake and ocean acidification in the North Atlantic Ocean. *Biogeosciences*, 9(7), 2509–2522. <https://doi.org/10.5194/bg-9-2509-2012>
- Bauer, J. E., Cai, W.-J., Raymond, P. A., Bianchi, T. S., Hopkinson, C. S., & Regnier, P. A. G. (2013). The changing carbon cycle of the coastal ocean. *Nature*, 504(7478), 61–70. <https://doi.org/10.1038/nature12857>

## Acknowledgments

The authors would like to thank the Oak Ridge Institute for Science and Education for sponsoring this research. We would also like to thank Emily Whitney for her help collecting and maintaining the stream chemistry data from the Juneau Road System. The scientific results and conclusions, as well as any views or opinions expressed herein, are those of the author(s) and do not necessarily reflect those of NOAA or the Department of Commerce. Reference to trade names does not imply endorsement by the Auke Bay Laboratories, National Marine Fisheries Service, NOAA Fisheries, or the Department of Commerce. The research presented here was funded by the National Science Foundation Established Program to Stimulate Competitive Research (NSF-Alaska EPSCoR OIA-1757348) and the NSF Coastal Marine Research Coordination Network (DEB-1557186).



- Bianucci, L., Long, W., Khangaonkar, T., Pelletier, G., Ahmed, A., Mohamedali, T., et al. (2018). Sensitivity of the regional ocean acidification and carbonate system in Puget Sound to ocean and freshwater inputs. *Elementa: Science of the Anthropocene*, 6, 22. <https://doi.org/10.1525/elementa.151>
- Biles, F. E., Edwards, R. T., D'Amore, D. V., Fellman, J. B., Hood, E. W., Trubilowicz, J. W., & Floyd, W. C. (2021). *Data for "Riverine dissolved organic carbon and freshwater export in the eastern Gulf of Alaska"*. Forest Service Research Data Archive. <https://doi.org/10.2737/RDS-2020-0045>
- British Columbia Ministry of Forests, Lands, Natural Resource Operations and Rural Development (BC FLNRO). (2012). Freshwater Atlas Watershed Groups (FWWTRSHDGR) [Dataset]. Retrieved from <https://catalogue.data.gov.bc.ca/dataset/freshwater-atlas-watershed-groups>
- Butman, D., & Raymond, P. A. (2011). Significant efflux of carbon dioxide from streams and rivers in the United States. *Nature Geoscience*, 4(12), 839–842. <https://doi.org/10.1038/ngeo1294>
- Butman, D., Striegl, R., Stackpoole, S., del Giorgio, P., Prairie, Y., Pilcher, D., et al. (2018). *Chapter 14: Inland waters*. Second state of the carbon cycle report. U.S. Global Change Research Program. <https://doi.org/10.7930/SOCCR2.2018.Ch14>
- Campeau, A., Wallin, M. B., Giesler, R., Löfgren, S., Mörth, C.-M., Schiff, S., et al. (2017). Multiple sources and sinks of dissolved inorganic carbon across Swedish streams, refocusing the lens of stable C isotopes. *Scientific Reports*, 7(1), 9158. <https://doi.org/10.1038/s41598-017-09049-9>
- Chapman, D. L. (1982). *Daily flow statistics of Alaskan streams*, NOAA Technical Memorandum. National Weather Service.
- Curran, J. H., & Biles, F. E. (2021). Identification of seasonal streamflow regimes and streamflow drivers for daily and peak flows in Alaska. *Water Resources Research*, 57(2), e2020WR028425. <https://doi.org/10.1029/2020WR028425>
- De Cicco, L. A., Lorenz, D., Hirsch, R. M., & Watkins, W. (2018). dataRetrieval: R packages for discovering and retrieving water data available from U.S. Federal Hydrologic Web Services [Software]. United States Geological Survey. <https://doi.org/10.5066/P9X4L3GE>
- Doney, S. C., Fabry, V. J., Feely, R. A., & Kleypas, J. A. (2009). Ocean acidification: The other CO<sub>2</sub> problem. *Annual Review of Marine Science*, 1, 169–192. <https://doi.org/10.1146/annurev.marine.010908.163834>
- Drake, T. W., Raymond, P. A., & Spencer, R. G. M. (2018). Terrestrial carbon inputs to inland waters: A current synthesis of estimates and uncertainty. *Limnology and Oceanography Letters*, 3, 132–142. <https://doi.org/10.1002/lol2.10055>
- Driscoll, C. T., Fuller, R. D., & Schecher, W. D. (1989). The role of organic acids in the acidification of surface waters in the Eastern U.S. *Water, Air, and Soil Pollution*, 43(1–2), 21–40. <https://doi.org/10.1007/BF00175580>
- Duarte, C. M., Hendriks, I. E., Moore, T. S., Olsen, Y. S., Steckbauer, A., Ramajo, L., et al. (2013). Is ocean acidification an open-ocean syndrome? Understanding anthropogenic impacts on seawater pH. *Estuaries and Coasts*, 36(2), 221–236. <https://doi.org/10.1007/s12237-013-9594-3>
- Edwards, R. T., D'Amore, D. V., Biles, F. E., Fellman, J. B., Hood, E. W., Trubilowicz, J. W., & Floyd, W. C. (2021). Riverine dissolved organic carbon and freshwater export in the eastern Gulf of Alaska. *Journal of Geophysical Research: Biogeosciences*, 126(1), e2020JG005725. <https://doi.org/10.1029/2020JG005725>
- Edwards, R. T., D'Amore, D. V., Norberg, E., & Biles, F. (2013). Riparian ecology, climate change, and management in North Pacific coastal rainforests. In G. H. Orians & J. W. Schoen (Eds.), *North Pacific temperate rainforests: Ecology and conservation* (pp. 43–72). University of Washington Press. Retrieved from <http://www.jstor.org/stable/j.ctvcwn56w.6>
- Evans, W., Lebon, G. T., Harrington, C. D., Takeshita, Y., & Bidlack, A. (2022). Marine CO<sub>2</sub> system variability along the northeast Pacific Inside Passage determined from an Alaskan ferry. *Biogeosciences*, 19(4), 1277–1301. <https://doi.org/10.5194/bg-19-1277-2022>
- Gattuso, J.-P., Epitalon, J.-M., Lavigne, H., & Orr, J. (2018). seacarb: Seawater carbonate chemistry. R package [Software]. U.S. Geological Survey. Retrieved from <https://CRAN.R-project.org/package=seacarb>
- Genet, H., He, Y., Lyu, Z., McGuire, A. D., Zhuang, Q., Clein, J., et al. (2018). The role of driving factors in historical and projected carbon dynamics of upland ecosystems in Alaska. *Ecological Applications*, 28(1), 5–27. <https://doi.org/10.1002/eap.1641>
- Gislason, S. R., Oelkers, E. H., Eiriksdottir, E. S., Kardjilov, M. I., Gisladottir, G., Sigfusson, B., et al. (2009). Direct evidence of the feedback between climate and weathering. *Earth and Planetary Science Letters*, 277(1–2), 213–222. <https://doi.org/10.1016/j.epsl.2008.10.018>
- Godsey, S. E., Hartmann, J., & Kirchner, J. W. (2019). Catchment chemostasis revisited: Water quality responds differently to variations in weather and climate. *Hydrological Processes*, 33(24), 3056–3069. <https://doi.org/10.1002/hyp.13554>
- Gomez, F. A., Wanninkhof, R., Barbero, L., & Lee, S.-K. (2021). Increasing river alkalinity slows ocean acidification in the northern Gulf of Mexico. *Geophysical Research Letters*, 48(24), e2021GL096521. <https://doi.org/10.1029/2021GL096521>
- Guo, J., Wang, F., Vogt, R. D., Zhang, Y., & Liu, C.-Q. (2015). Anthropogenically enhanced chemical weathering and carbon evasion in the Yangtze Basin. *Scientific Reports*, 5(1), 11941. <https://doi.org/10.1038/srep11941>
- Harley, J. R., Biles, F. E., Brooks, M. K., Fellman, J. B., Hood, E. W., & D'Amore, D. V. (2022). Juneau river stream chemistry and discharge for calculation of inorganic carbon flux [Dataset]. Forest Service Research Data Archive. <https://doi.org/10.2737/RDS-2022-0058>
- Hauri, C., Schultz, C., Hedstrom, K., Danielson, S., Irving, B., Doney, S. C., et al. (2020). A regional hindcast model simulating ecosystem dynamics, inorganic carbon chemistry, and ocean acidification in the Gulf of Alaska. *Biogeosciences*, 17(14), 3837–3857. <https://doi.org/10.5194/bg-17-3837-2020>
- Hood, E., Fellman, J. B., & Spencer, R. G. M. (2020). Glacier loss impacts riverine organic carbon transport to the ocean. *Geophysical Research Letters*, 47(19), e2020GL089804. <https://doi.org/10.1029/2020GL089804>
- Jarvie, H. P., King, S. M., & Neal, C. (2017). Inorganic carbon dominates total dissolved carbon concentrations and fluxes in British rivers: Application of the THINCARB model – Thermodynamic modelling of inorganic carbon in freshwaters. *Science of the Total Environment*, 575, 496–512. <https://doi.org/10.1016/j.scitotenv.2016.08.201>
- Larsen, C. F., Motyka, R. J., Freymueller, J. T., Echelmeyer, K. A., & Ivins, E. R. (2005). Rapid viscoelastic uplift in southeast Alaska caused by post-Little Ice Age glacial retreat. *Earth and Planetary Science Letters*, 237(3–4), 548–560. <https://doi.org/10.1016/j.epsl.2005.06.032>
- Lê, S., Josse, J., & Husson, F. (2008). FactoMineR: An R package for multivariate analysis. *Journal of Statistical Software*, 25, 1–18. <https://doi.org/10.18637/jss.v025.i01>
- Leighty, W. W., Hamburg, S. P., & Caouette, J. (2006). Effects of management on carbon sequestration in forest biomass in southeast Alaska. *Ecosystems*, 9(7), 1051–1065. <https://doi.org/10.1007/s10021-005-0028-3>
- Lesnek, A. J., Briner, J. P., Baichtal, J. F., & Lyles, A. S. (2020). New constraints on the last deglaciation of the Cordilleran Ice Sheet in coastal Southeast Alaska. *Quaternary Research*, 96, 140–160. <https://doi.org/10.1017/qua.2020.32>
- Li, M., Peng, C., Wang, M., Xue, W., Zhang, K., Wang, K., et al. (2017). The carbon flux of global rivers: A re-evaluation of amount and spatial patterns. *Ecological Indicators*, 80, 40–51. <https://doi.org/10.1016/j.ecolind.2017.04.049>
- Manizza, M., Follows, M. J., Dutkiewicz, S., McClelland, J. W., Menemenlis, D., Hill, C. N., et al. (2009). Modeling transport and fate of riverine dissolved organic carbon in the Arctic Ocean. *Global Biogeochemical Cycles*, 23(4), GB4006. <https://doi.org/10.1029/2008GB003396>
- McCabe, G. J., & Markstrom, S. L. (2007). *A monthly water-balance model driven by a graphical user interface*. US Geological Survey Reston.

- McNicol, G., Bulmer, C., D'Amore, D., Sanborn, P., Saunders, S., Giesbrecht, I., et al. (2019). Large, climate-sensitive soil carbon stocks mapped with pedology-informed machine learning in the North Pacific coastal temperate rainforest. *Environmental Research Letters*, *14*(1), 014004. <https://doi.org/10.1088/1748-9326/aaed52>
- Milner, A. M., Khamis, K., Battin, T. J., Brittain, J. E., Barrand, N. E., Füreder, L., et al. (2017). Glacier shrinkage driving global changes in downstream systems. *Proceedings of the National Academy of Sciences*, *114*(37), 9770–9778. <https://doi.org/10.1073/pnas.1619807114>
- Moore, R. D., Trubilowicz, J. W., & Buttle, J. M. (2012). Prediction of streamflow regime and annual runoff for ungauged basins using a distributed monthly water balance model. *Journal of the American Water Resources Association*, *48*(1), 32–42. <https://doi.org/10.1111/j.1752-1688.2011.00595.x>
- Nash, J. E., & Sutcliffe, J. V. (1970). River flow forecasting through conceptual models part I – A discussion of principles. *Journal of Hydrology*, *10*(3), 282–290. [https://doi.org/10.1016/0022-1694\(70\)90255-6](https://doi.org/10.1016/0022-1694(70)90255-6)
- Neal, E. G., Hood, E., & Smikrud, K. (2010). Contribution of glacier runoff to freshwater discharge into the Gulf of Alaska. *Geophysical Research Letters*, *37*(6), L06404. <https://doi.org/10.1029/2010GL042385>
- OpenTopography. (2020). NASA Shuttle Radar Topography Mission (SRTM) (2013) [Dataset]. Shuttle Radar Topography Mission (SRTM) Global. <https://doi.org/10.5069/G9445JDF>
- Orr, J. C., Fabry, V. J., Aumont, O., Bopp, L., Doney, S. C., Feely, R. A., et al. (2005). Anthropogenic ocean acidification over the twenty-first century and its impact on calcifying organisms. *Nature*, *437*(7059), 681–686. <https://doi.org/10.1038/nature04095>
- Parde, M. (1933). Fleuves et rivières. Collection Armand Colin. Section de Géographie (France) fr no. 155.
- Prokushkin, A. S., Pokrovsky, O. S., Shirokova, L. S., Korets, M. A., Viers, J., Prokushkin, S. G., et al. (2011). Sources and the flux pattern of dissolved carbon in rivers of the Yenisey basin draining the Central Siberian Plateau. *Environmental Research Letters*, *6*(4), 045212. <https://doi.org/10.1088/1748-9326/6/4/045212>
- Punt, A. E., Poljak, D., Dalton, M. G., & Foy, R. J. (2014). Evaluating the impact of ocean acidification on fishery yields and profits: The example of red king crab in Bristol Bay. *Ecological Modelling*, *285*, 39–53. <https://doi.org/10.1016/j.ecolmodel.2014.04.017>
- R Core Team. (2023). R: A language and environment for statistical computing [Software]. R Foundation for Statistical Computing. Retrieved from <https://www.R-project.org/>
- Raymond, P. A., Hartmann, J., Lauerwald, R., Sobek, S., McDonald, C., Hoover, M., et al. (2013). Global carbon dioxide emissions from inland waters. *Nature*, *503*(7476), 355–359. <https://doi.org/10.1038/nature12760>
- Runkel, R. L., Crawford, C. G., & Cohn, T. A. (2004). *Load estimator (LOADEST): A FORTRAN program for estimating constituent loads in streams and rivers (USGS numbered series no. 4-A5)*. Techniques and Methods. U.S. Geological Survey, Reston. <https://doi.org/10.3133/tm4A5>
- Savoie, A. M., Moody, A., Gilbert, M., Dillon, K. S., Howden, S. D., Shiller, A. M., & Hayes, C. T. (2022). Impact of local rivers on coastal acidification. *Limnology & Oceanography*, *67*(12), 2779–2795. <https://doi.org/10.1002/lno.12237>
- Sergeant, C. J., Falke, J. A., Bellmore, R. A., Bellmore, J. R., & Crumley, R. L. (2020). A classification of streamflow patterns across the coastal Gulf of Alaska. *Water Resources Research*, *56*(2), e2019WR026127. <https://doi.org/10.1029/2019WR026127>
- Shanley, C. S., & Albert, D. M. (2014). Climate change sensitivity index for Pacific salmon habitat in Southeast Alaska. *PLoS One*, *9*(8), e104799. <https://doi.org/10.1371/journal.pone.0104799>
- Shulski, M., & Wendler, G. (2007). *The climate of Alaska*. University of Alaska Press.
- Siedlecki, S. A., Pilcher, D. J., Hermann, A. J., Coyle, K., & Mathis, J. (2017). The importance of freshwater to spatial variability of aragonite saturation state in the Gulf of Alaska. *Journal of Geophysical Research: Oceans*, *122*(11), 8482–8502. <https://doi.org/10.1002/2017JC012791>
- Sowa, J. (2013). *Peterson Creek streamgage, 2012–2018 (Regional Operational Plan No. SF.4A.2013.04)*. Alaska Department of Fish and Game.
- Stackpoole, S., Butman, D., Clow, D., Verdin, K., Gaglioti, B., & Striegl, R. (2016). Chapter 8. Carbon burial, transport, and emission from inland aquatic ecosystems in Alaska. In Z. Zhu & A. David McGuire (Eds.), *Baseline and projected future carbon storage and greenhouse-gas fluxes in ecosystems of Alaska*.
- Stackpoole, S. M., Butman, D. E., Clow, D. W., Verdin, K. L., Gaglioti, B. V., Genet, H., & Striegl, R. G. (2017). Inland waters and their role in the carbon cycle of Alaska. *Ecological Applications*, *27*(5), 1403–1420. <https://doi.org/10.1002/eap.1552>
- Steinacher, M., Joos, F., Frölicher, T. L., Plattner, G.-K., & Doney, S. C. (2009). Imminent ocean acidification in the Arctic projected with the NCAR global coupled carbon cycle-climate model. *Biogeosciences*, *6*(4), 515–533. <https://doi.org/10.5194/bg-6-515-2009>
- Stokes, T. R., & Griffiths, P. A. (2019). An overview of the karst areas in British Columbia, Canada. *Geoscience Canada: Journal of the Geological Association of Canada/Geoscience Canada: journal de l'Association Géologique du Canada*, *46*, 49–66. <https://doi.org/10.12789/geocanj.2019.46.145>
- Tank, S. E., Raymond, P. A., Striegl, R. G., McClelland, J. W., Holmes, R. M., Fiske, G. J., & Peterson, B. J. (2012). A land-to-ocean perspective on the magnitude, source and implication of DIC flux from major Arctic rivers to the Arctic Ocean. *Global Biogeochemical Cycles*, *26*(4). <https://doi.org/10.1029/2011GB004192>
- Tank, S. E., Striegl, R. G., McClelland, J. W., & Kokelj, S. V. (2016). Multi-decadal increases in dissolved organic carbon and alkalinity flux from the Mackenzie drainage basin to the Arctic Ocean. *Environmental Research Letters*, *11*(5), 054015. <https://doi.org/10.1088/1748-9326/11/5/054015>
- Torres, M. A., Moosdorf, N., Hartmann, J., Adkins, J. F., & West, A. J. (2017). Glacial weathering, sulfide oxidation, and global carbon cycle feedbacks. *PNAS*, *114*(33), 8716–8721. <https://doi.org/10.1073/pnas.1702953114>
- US Department of Commerce. (2023). Coastal marine zones [Dataset]. Retrieved from <https://www.weather.gov/gis/CoastalMarineMetadata>
- U.S. Geological Survey. (2023). *National Water Information System data available on the world wide web*. USGS Water Data for the Nation.
- USDA Forest Service, Tongass National Forest. (2021). Tongass National Forest Karstlands [Dataset]. US Forest Service. Retrieved from [https://gis.data.alaska.gov/datasets/01818a0f66bf4a42ba25ee5a0c94ee21\\_0/about](https://gis.data.alaska.gov/datasets/01818a0f66bf4a42ba25ee5a0c94ee21_0/about)
- Wang, T., Hamann, A., Spittlehouse, D. L., & Muddock, T. Q. (2012). ClimateWNA—High-resolution spatial climate data for western North America. *Journal of Applied Meteorology and Climatology*, *51*(1), 16–29. <https://doi.org/10.1175/JAMC-D-11-043.1>
- Waters, J., Millero, F. J., & Woosley, R. J. (2014). Corrigendum to “The free proton concentration scale for seawater pH”. *Marine Chemistry*, *165*, 66–67. <https://doi.org/10.1016/j.marchem.2014.07.004>
- Watershed Boundary Dataset (WBD). (2012). The watershed boundary dataset (WBD). Coordinated effort between the United States Department of Agriculture-Natural Resources Conservation Service (USDA-NRCS), the United States Geological Survey (USGS), and the Environmental Protection Agency (EPA).
- Weingartner, T., Eisner, L., Eckert, G. L., Danielson, S., & Bellwood, D. (2009). Southeast Alaska: Oceanographic habitats and linkages. *Journal of Biogeography*, *36*(3), 387–400. <https://doi.org/10.1111/j.1365-2699.2008.01994.x>